The Journal of Chemical Physics ARTICLE scitation.org/journal/jcp

Observation of the two-photon transition enhanced first hyperpolarizability spectra in cinnamaldehyde derivatives: A femtosecond regime study

Cite as: J. Chem. Phys. 158, 214201 (2023); doi: 10.1063/5.0151622
Submitted: 23 March 2023 • Accepted: 11 May 2023 •
Published Online: 1 June 2023

Carlos H. D. dos Santos,[1] Leandro H. Zucolotto Cocca,[1] André Gasparotto Pelosi,[1] Vasco F. Batista,[2] Diana C. G. A. Pinto,[2] M. Amparo F. Faustino,[2] Marcelo G. Vivas,[3] Jonathas de Paula Siqueira,[4] Cleber R. Mendonça,[1] and Leonardo De Boni[1,a)]

AFFILIATIONS

[1]Instituto de Física de São Carlos, Universidade de São Paulo, CP 369, 13560-970 São Carlos, Sao Paulo, Brazil
[2]LAQV-REQUIMTE, Department of Chemistry, University of Aveiro, 3810-193 Aveiro, Portugal
[3]Laboratório de Espectroscopia Óptica e Fotônica, Universidade Federal de Alfenas, Poços de Caldas, Minas Gerais, Brazil
[4]Instituto de Física Gleb Wataghin, Universidade Estadual de Campinas, Campinas, Sao Paulo, Brazil

[a)]**Author to whom correspondence should be addressed:** deboni@ifsc.usp.br

ABSTRACT

The application of nonlinear optical effects in optoelectronic devices is still scarce because the irradiance threshold necessary to induce a specific effect is very high. In this context, knowing the frequency-resolved first order molecular hyperpolarizability (β) is essential to identifying regions where this response is intense enough to allow for applications in commercial devices. Thus, herein, we have determined the β spectral dependence of five new push–pull cinnamylidene acetophenone derivatives using femtosecond laser-induced Hyper-Rayleigh Scattering (HRS). A considerable increase in β values was observed in molecules. We found remarkable β values in regions near the two-photon resonance, which are mediated by electron withdrawing and donating groups. This effect was mapped using wavelength-tunable femtosecond Z-scan technique. Furthermore, it was modeled in light of the sum-over-states approach for the second- and third-order nonlinearities. Finally, our outcomes suggest a strategy to obtain large β values mediated by the 2PA transition.

I. INTRODUCTION

First-order molecular hyperpolarizability spectral dependence [β(λ)] in organic molecules is essential for designing new photonics, optoelectronics, and nonlinear optical devices.[1–8] Nevertheless, the dispersion of β has been rarely explored in the literature from an experimental and theoretical point of view.[9–11] Theoretical studies are important to preview β(λ) values and support the experimental data.[12–14] Most of the experimental studies employing Hyper-Rayleigh Scattering (HRS) technique[15–17] were performed only for one excitation wavelength.[15,16,18,19] However, some papers report the spectral dependence with a nanosecond pulsed laser, which tends to induce spurious effects.[20–22] From these, Zhu *et al.*[22] were among the few who studied the spectral dependence of β in azobenzene (push–pull derivatives) and described the enhancement concerning the molecular shape performed by a nanosecond pulsed laser. In other words, β(λ) values obtained from femtosecond laser-induced HRS are still scarcer. Theoretical–experimental studies aim to understand and predict molecular structure–property relationships, specifically regarding β values that could be used to develop new molecular structures.[23,24] Furthermore, a significant increase in β values has been observed in chromophores with asymmetric structures and systems with long conjugated chains, for instance, aromatic and heteroaromatic rings (π–bridge) with electron-donating (ED) and electron-withdrawing (EW) groups grafted to them (D-π-A structures). More complex architectures, such as quadruple or octopolar branched structures[25,26] and non-centrosymmetric semiconductor nanocrystals,[27] are promising materials to present high values of β.

Cinnamylidene acetophenone (CA) derivatives are precursors in synthesizing molecules with potential biological activity. Their molecular structure is similar to curcumin, which is a natural polyphenol considered a safe phytochemical. Curcumin presents several pharmacological properties, such as anti-inflammatory, anticancer, and antioxidant activities.[28–36] Furthermore, this type of molecular structure may be of great interest for nonlinear optical applications due to its high synthesis flexibility in terms of π-conjugation length and addition of electron-withdrawing (EW) and electron-donating (ED) groups,[37,38] which may increase its nonlinear optical response. However, there is a lack of literature on the nonlinear optical features of CA derivatives.

Therefore, this work represents a significant advancement in understanding the relationship between molecular structure and its potential for new nonlinear optical applications. In this context, spectral-resolved HRS technique was implemented to describe the β dispersion for five CA derivatives. From the experimental spectra of β, we observed a two-photon transition enhanced HRS signal (around 700 nm) for all molecules. Theoretically, the β signal presents one-photon (1PA) and two-photon absorption (2PA) allowed resonances.[39] In several studies, the 1PA resonances have been used as a strategy to obtain large nonlinear optical effects.[25,40] However, 2PA-allowed resonances are little explored because there is a lack of information in the literature on the β dispersion. Herein, we noticed that 2PA enhanced β values are one order of magnitude larger than in the region far from the two-photon resonance (1200 nm). In addition, our outcomes show as the strength of EW and ED groups played a fundamental role in the first-order molecular hyperpolarizability magnitude of the studied molecules. Consequently, the scattered molecular second harmonic spectra have a global linear increasing tendency with the charge group strengths.[41]

As complementary analyses for β, a modeling approach based on the Sum-Over-States (SOS) model was used. In this case, we connect molecular photophysical parameters obtained from the 1PA and 2PA spectra to describe the β dispersion and the enhancement effect caused by the 2PA resonance. Moreover, the experimental data obtained by wavelength-resolved HRS technique (β values spectra) and the 2PA cross-sectional values showed excellent agreement with the phenomenological models applied.

II. EXPERIMENTAL DETAILS

Details of the synthesis can be found in Refs. 42 and 43. The nomenclature of the five CA molecules studied here, see Fig. 1, is (E,E)-cinnamylidene acetophenones (**C1**), (E,E)-4′-fluorocinnamylidene acetophenones (**C2**), (E,E)-4′-bromocinnamylidene acetophenones (**C3**), (E,E)-4′-cyanocinnamylidene acetophenones (**C4**), and (E,E)-4′ methyl cinnamylidene acetophenones (**C5**).

All samples used in this work were dissolved in pure dimethyl sulfoxide (DMSO—P.A). The difference between CA derivatives is related to the elements of peripheral groups. The main molecular structure of CA derivatives can be described as two aromatic rings joined by a carbonyl α,β,γ,δ unsaturated five-carbon. Beyond the π-conjugated bridge, which leads to an increase in the nonlinear optical response, the molecules C2, C3, and C4 all have EW atoms

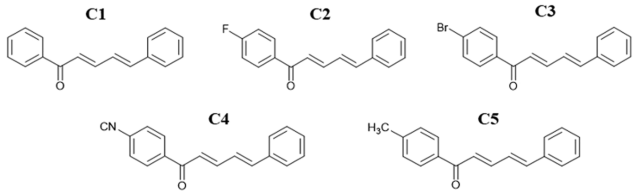

FIG. 1. CA derivatives of a chemical molecular structure. The five molecules differ by the peripheral groups attached to the left side of the phenyl group.

(F, Br, and CN), with only C5 having an ED group (CH_3) bound in the phenyl group in the *para* position. As a result, these molecules can be treated as dipolar structures of the A-π-D and D-π-D types, respectively.

A. One- and two-photon absorption measurements

For 1PA measurements, a commercial SHIMADZU UV-1800 spectrometer was used. All samples were dissolved in DMSO at ~10^{-4} mol/L concentrations. A quartz cuvette with an optical path of 1 mm was used to measure the linear absorption spectrum. No fluorescence was observed for all the CA derivatives using a commercial HITACHI F-7000 fluorimeter and concentrations on the order of 10^{-5} mol/L. For 2PA measurements, frequency-resolved femtosecond open aperture Z-scan technique was carried out (experimental details are presented in the supplementary material, Sec. 1). 1PA and 2PA measurements were performed to determine the photophysical parameters in order to simulate the first order molecular hyperpolarizability dispersion.

B. Tunable femtosecond HRS technique

Femtosecond tunable HRS technique implemented employs an optical parametric amplifier (Orpheus—Light Conversion) pumped by an amplified femtosecond laser system (Pharos—Light Conversion, 1030 nm, 190 fs, 7.5 kHz) as tunable laser excitation, allowing for tuning from visible to near-infrared. A schematic figure of the experimental setup used to perform HRS measurements is illustrated in Fig. 2. An automated rotation stage controls the λ/2 broadband waveplate that, combined with two polarizers, provides beam power control while keeping the vertical polarization of the light electric field. A λ/2 beam splitter separates a portion (<4%) of the beam to a *silicon or germanium* reference photodetector. A cylindrical lens was used to increase the irradiation area and, consequently, the number of scattering centers.

Due to the very low intensity of the HRS signal,[44] a photomultiplier (PMT) is employed, combined with a lens telescope and a concave spherical mirror. A long-pass filter was used at the entrance of a dark box, allowing only the incident wavelength beam to pass through. As a result of one measurement of HRS, a typical curve of the scattered molecular second harmonic signal [I(2ω)] is obtained as a function of incident beam intensity [I(ω)] for each frequency ω. Each experimental point of the curve is averaged over ~10k laser pulses using two lock-in amplifiers, one for the reference detector and the other for the PMT signal, increasing the signal-to-noise ratio.

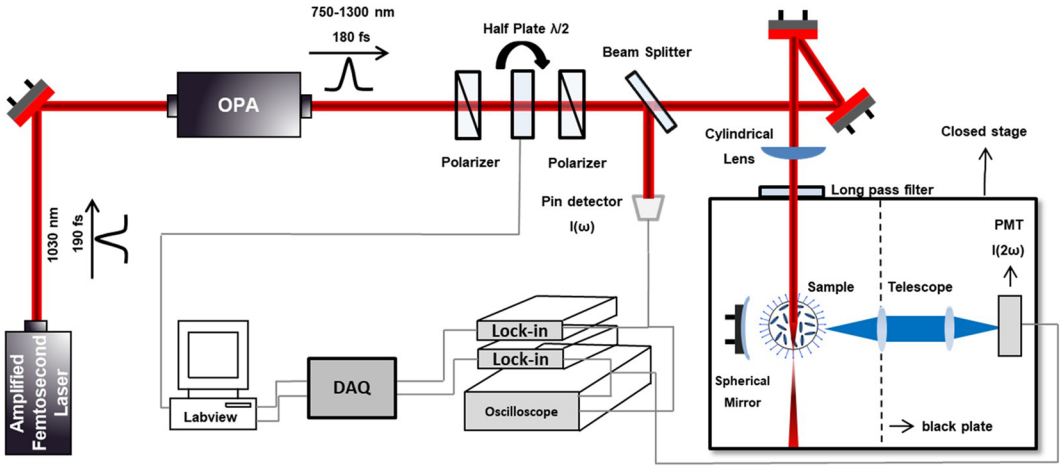

FIG. 2. Schematic of the experimental optical setup of the tunable hyper-Rayleigh scattering for the measurement of the first order molecular hyperpolarizability β.

C. Determining the dispersion of first-order hyperpolarizability by external reference method (ERM)

Employing the ERM to determine the magnitude of the first-order hyperpolarizability[45,46] (see more details about the methodology in the supplementary material, Sec. 2), several measurements were performed considering the reference sample and CA derivatives, both dissolved in pure DMSO. As an example of typical HRS experimental curves, in Fig. 3(a), one can see the quadratic dependence of I(2ω) with I(ω) for several C3 concentrations, measured with an incident laser beam at 850 nm. In addition, in Fig. 3(b), the quadratic coefficients $[I(2\omega)/I^2(\omega)]$ are plotted as a function of the C3, C4, and pNA concentration, showing a linear behavior expected for this measurement. The linear fits (solid lines) return the slopes with *para*-nitroaniline (pNA) as the reference sample. The measurements were performed over a range from 750 to 1200 nm with 50 nm intervals, and the values of β(λ) for pNA were obtained from the work of Sciuti *et al.*[47]

III. RESULTS AND DISCUSSIONS

Figure 4 shows the 1PA (solid lines) and β(λ) (symbols, measured from 750 nm up to 1200 nm with steps of 50 nm for all five cinnamaldehyde derivatives). The 1PA spectra show that all samples are transparent for wavelengths longer than 420 nm, demonstrating that there is not any 1PA in the region in which the HRS experiments were performed. In addition, one can see a lower energy absorption band located at 350 nm for all derivatives, which is related to the longer molecular conjugated part of the derivatives, in this case the cinnamylidene. Disregarding C1, the other samples present an extra absorption band at *c.a.* 270 nm, which is caused by the presence of the EW and ED on the acetophenone side. The maximum molar absorption coefficient (ε) is around 30 000 M^{-1} cm^{-1} for the lowest energy absorption band, observed in all molecules. For the second absorption band, ε ranges from ~9000 to 18 000 M^{-1} cm^{-1}, according to the strength of the ED or EW groups. As mentioned before, all samples do not show any presence of fluorescence emission.

Furthermore, the β(λ) values tend to increase as the wavelength of the laser becomes closer to the absorption of the molecule. Indeed, a monotonic growth in β magnitude is observed from the IR going into the visible region for all samples. One can note that for wavelengths shorter than 850 nm, β increases considerably when compared to the rest. These wavelengths are twice the 1PA wavelengths, which may indicate that the second harmonic generated is being enhanced by a two-photon allowed transition at this region.

The largest β values for all molecules are observed at 750 nm. It is possible to note that the molecules containing the ED or EW groups also have higher values when compared to the C1 molecule without any group. The largest value observed in C4 is approximately two times greater than C1. In addition, when excited around 1200 nm, all molecules slightly increase the β magnitude when compared to C1. Both features are further explained based on the sample's energy-essential electronic states.

The increase in β values for all derivatives compared to C1 can be understood by the presence of the two 1PA bands. C1 has only one 1PA band at the same region and the lowest β magnitudes. Regarding C2, C3, C4, and C5, the enhancement of the molecular second harmonic scattering may be attributed to the higher energy band magnitude, which depends on the EW or ED groups bound to phenyl. The presence of the higher energy band is directly related to a decrease in the charge symmetry at the acetophenone molecule, originating an extra coupling between the radiation and the molecules. This effect will be visualized by using the SOS approach.

To shed more light on the results, we have employed the sum over essential states approach to describe the experimental first-order hyperpolarizability spectra[37] considering two- (fundamental state and one excited state—2LM) and three-level systems (one fundamental state and two excited states—3LM),[47–50] respectively, for C1 and the other molecules. Whereas all studied molecules present

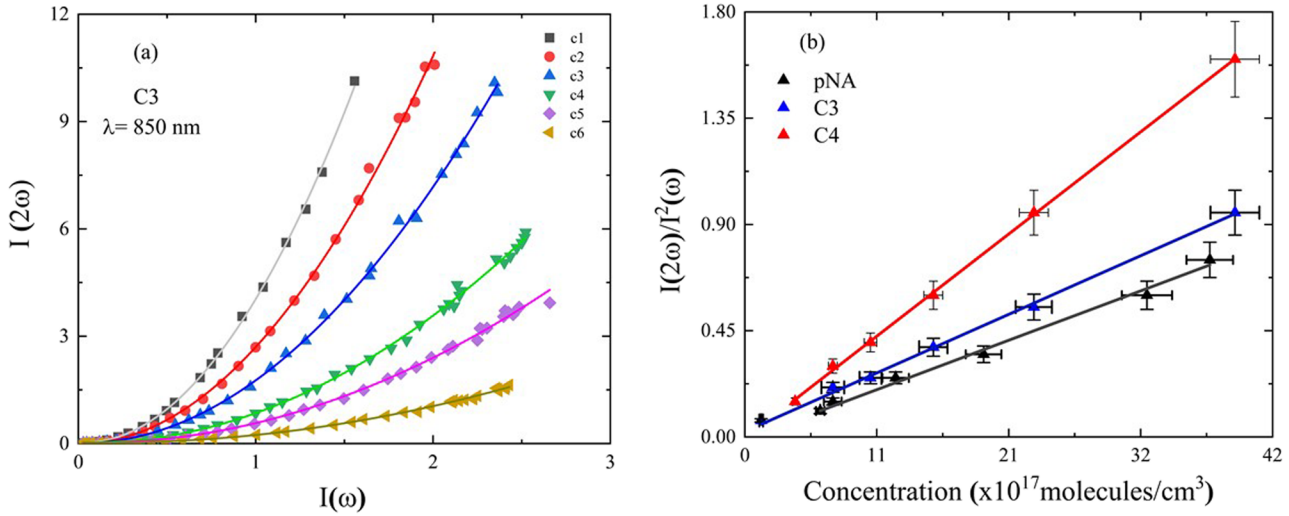

FIG. 3. (a) One example of the measurements of I(2ω) vs I(ω) and their respective quadratic fits for molecule C3 as a function of concentration, measured at 850 nm, in which C1 is the most concentrated solution. (b) The linear dependence of the quadratic coefficient with sample concentration for pNA, C3, and C4 at the same wavelength. Both error bars were estimated at 10%.

C_{2v}-like symmetry (depolarization ratio $\rho = \frac{\langle\beta^2_{xzz}\rangle}{\langle\beta^2_{zzz}\rangle} = \frac{1}{5}$), in which the most uniaxial dipolar molecules with the z axis being the molecular dipole axis and, consequently, the β_{zzz} component is much larger than β_{zxx}.[51,52] As the experimental HRS for all molecules was obtained from 1200 to 750 nm, a simplified equation considering the complete model described in Ref. 37 was used for the 2LM approach,

$$\beta_{2LM}(\omega,\omega_{01},\Gamma_{01}) = \left[\frac{3{\mu_{01}}^2\Delta\mu_{01}}{2(\hbar\omega_{01})^2}\right]\left[\left(\frac{1}{3}\frac{\omega_{01}}{[(\omega_{01}-\omega)-i\Gamma_{01}]} \times \frac{\omega_{01}}{[(\omega_{01}-2\omega)-i\Gamma_{01}]}\right)\right] = \left[\frac{3{\mu_{01}}^2\Delta\mu_{01}}{2(\hbar\omega_{01})^2}\right]\left[\left(\frac{1}{3}R_{1PA}R_{2PA}\right)\right], \quad (1)$$

in which the quantities in the first square brackets define the static first-order molecular hyperpolarizability β_0, while the second represents the dynamical one that presents 1PA and 2PA allowed resonances (R_{1PA} and R_{2PA}). In Eq. (1), μ_{01} is the transition dipole moment from the ground state to the first excited state, $\Delta\mu_{01}$ is the difference between the permanent ground state dipole moment and the first excited state one, $\hbar$ is Planck's constant divided by 2π, ω_{01} is the transition frequency related to the ground state (0) to the first excited state (1), Γ_{01} is the half-width at half-maximum of the first excited state absorption band, and ω is the laser incident frequency. For the 3LM, the modeling equation is similar to Eq. (1), but with an extra term added related to the second absorption band.[37] Again, in this case, the dynamic microscopic first-order hyperpolarizability, from 1200 to 750 nm, is given by simplified 3LM considering only two components of the sum-over-essential states.[37] All details of simplification were described in Sec. 5 of the supplementary material, so:

$$\beta_{3LM}(\omega,\omega_{01},\Gamma_{01},\omega_{02},\Gamma_{02}) = \beta_{2LM}(\omega,\omega_{01},\Gamma_{01}) + \frac{3\mu_{01}\mu_{02}\mu_{12}}{2(\hbar\omega_{01})(\hbar\omega_{02})} \times \left[\frac{1}{3}\left(R_{2PA}\frac{(\omega_{02})}{(\omega_{02}-\omega-i\Gamma_{02})}\right)\right], \quad (2)$$

in which the extra term brings additional photophysical parameters associated with the second absorption band: μ_{02} is the transition dipole moment from the ground state to the second excited state, μ_{12} is the transition dipole moment from the first state to the second excited state, ω_{02} is the transition frequency related to the ground state (0) to the second excited state (2), and Γ_{02} is the half-width at half-maximum referred to as the electronic transition ($0 \rightarrow 2$). As can be seen in Eqs. (1) and (2), it is necessary to know some photophysical parameters to simulate the first-order molecular hyperpolarizability dispersion.

In this manner, most of the input photophysical parameters are obtained by carefully analyzing 1PA and 2PA spectroscopies: the transition dipole moments (μ_{01}, μ_{02}), defined by the absorption bands according to Eq. (SI6); the central transition frequencies (ω_{01} and ω_{02}), obtained from the maximum absorption value of the respective bands; and the line broadenings determined by FWHM of the first and second excited states of absorption bands, respectively (ranging from 0.3 to 0.5 eV). All these parameters were determined from 1PA spectroscopy. More details are found in the supplementary material, Sec. 3. As can be noted in Eq. (1), $\Delta\mu_{01}$ is known not only from 1PA measurements but can be from 2PA spectroscopy. We used open-aperture Z-scan technique to measure the 2PA cross-sectional spectra [σ_{2PA} (λ)], shown as open circles in Fig. 5 and Fig. SI-2. More details can be found in the supplementary material.

Regarding the 2PA spectra, C1 depicts only one 2PA band, and all the other ones have two 2PA bands, all mirroring the same position of the 1PA bands (red dashed lines), an indication that the 1PA bands are also 2PA-allowed for all molecules. The maximum value

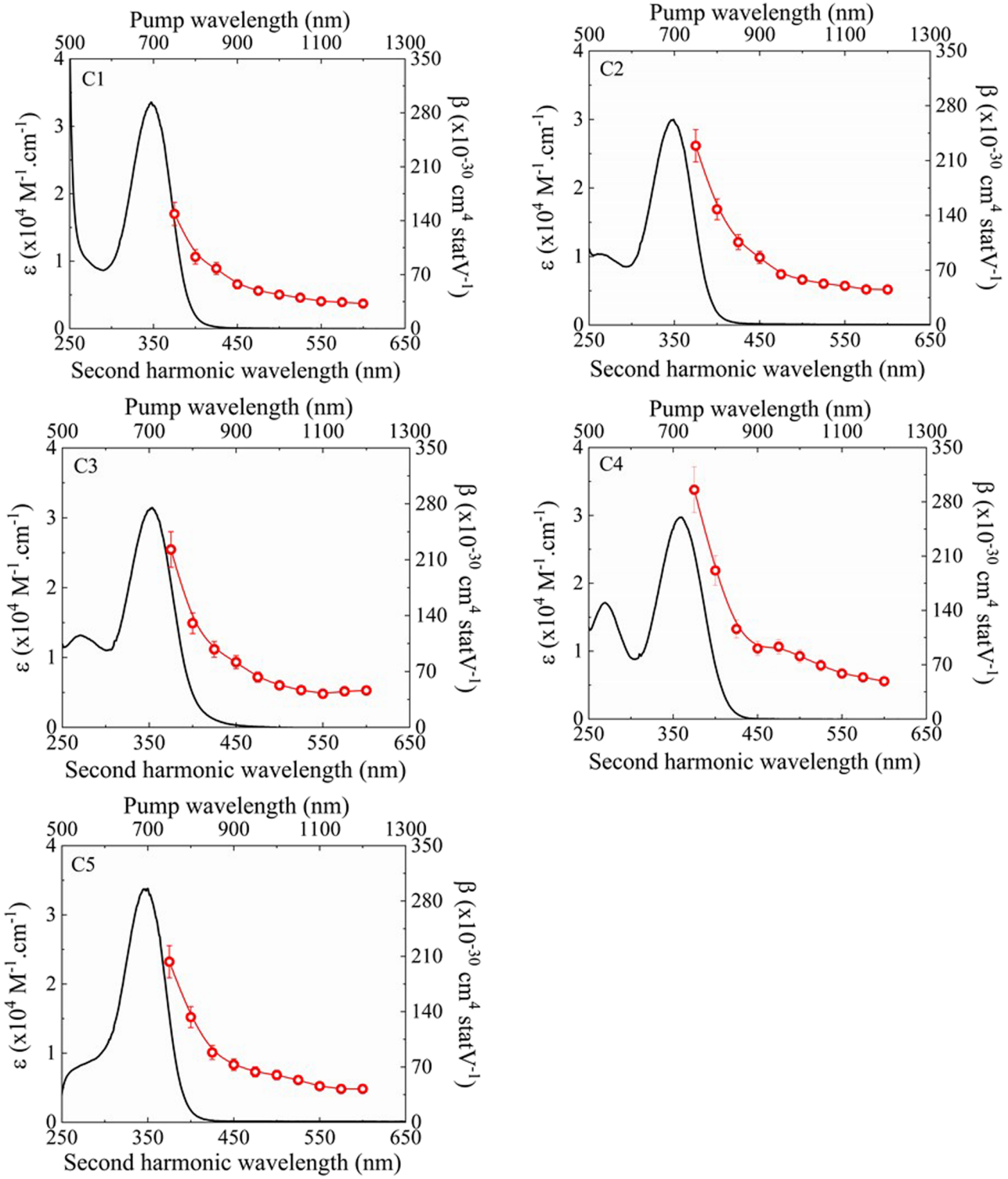

FIG. 4. The red circles represent the dispersion of the first-order hyperpolarizability β for the five CA derivatives obtained by HRS femtosecond technique with a red solid line only to guide. The black solid lines show the 1PA spectra.

of the 2PA related to the lower energy band (~350 nm) is around 30 GM for all samples, which is in accordance with the ones observed in similar molecular structures.[45,53,54] Concerning the second 2PA state (~270 nm), the maximum 2PA cross-sectional values are slightly higher than the ones observed in the first excited state. It can be seen by comparing the 1PA and 2PA in Fig. 5, for the C4 molecule, for example. In addition, between C1 and C4 molecules, only one 1PA and 2PA bands are observed for C1; it can be understood due to the lack of peripheral groups.

The magnitude of the 2PA cross section for the higher energy band significantly increases depending on the peripheral atom attached to the phenyl group. This variation is due to the strength of the EW or ED groups, which optimizes nonlinear optical responses.[55] It results in a considerable increment in the value of the higher energy state's transition dipole moment (μ_{02}). Therefore, our result shows the maximum magnitude of the 2PA cross section for the higher energy band as follows: $\sigma_{2PA}^{CN} > \sigma_{2PA}^{Br} > \sigma_{2PA}^{F} > \sigma_{2PA}^{CH_3}$ in accordance with the strength of EW/ED groups.

On the 2PA experimental spectra, we employ the SOS approach to extract the values of the difference between the permanent dipole moments of the ground and first excited states, the ground and second excited states, and the transition dipole moment between the first and second excited states, respectively, $\Delta\mu_{01}$, $\Delta\mu_{02}$, and μ_{12} for all molecules. The 2PA cross-sectional spectrum, for a non-centrosymmetric charge distribution, can be described (blue solid lines in Fig. 5 and Fig. SI-2) by using the following equation:[56]

$$\sigma_{2PA}(\omega) = \frac{2}{5}\frac{(2\pi)^4}{(chn)^2}L^4\frac{1}{\pi}\left[\frac{\Delta\mu_{01}^2\mu_{01}^2\Gamma_{01}}{(\omega_{01}-2\omega)^2+\Gamma_{01}^2} + \frac{\Delta\mu_{02}^2\mu_{02}^2\Gamma_{02}}{(\omega_{02}-2\omega)^2+\Gamma_{02}^2} + \frac{\omega^2}{(\omega_{01}-\omega)^2+\Gamma_{01}^2}\frac{\mu_{12}^2\mu_{01}^2\Gamma_{02}}{(\omega_{02}-2\omega)^2+\Gamma_{02}^2} + \frac{\Delta\mu_{02}\mu_{02}\mu_{01}\mu_{12}\Gamma_{02}}{(\omega_{02}-2\omega)^2+\Gamma_{02}^2}\right], \quad (3)$$

in which c is the speed of light, n is the DMSO linear refractive index (n = 1.4793), and L is Onsager's local field factor given by $L = 3n^2/(2n^2+1)$. All the terms inside of the square brackets were used to describe the first 2PA band (first term), the second 2PA (second term), the 1PA enhancement effect (third term), and the interference term between both excited states (fourth term). This complete equation was used to model all molecules except for C1, for which only the first term was employed due to the presence of only one 2PA band.

The photophysical parameters determined by 1PA and 2PA are displayed in Table I. For all molecules, μ_{01} shows similar values, which is expected because they were all determined from the first excited state band, which, according to the 1PA, has approximately the same molar absorptivity. The same can be seen for $\Delta\mu_{01}$ and $\Delta\mu_{02}$ values, which, respectively, are explained by the first and second 2PA bands, which present similar 2PA cross-sectional values for all molecules. For μ_{02}, which describes the transition dipole moment from the ground to the second excited state, it is possible to note, as cited before, an increase in the magnitude according to the strength of ED or EW groups. The lowest value is determined for C5, followed by C2, C3, and, finally, C4. This result demonstrates that both the magnitude of first-order molecular hyperpolarizability and the 2PA spectra have the same tendency.

With the photophysical parameters shown in Table I, we used Eqs. (1) and (2) to simulate the dispersion of β(λ) for all molecules from 600 up to 1300 nm. It is possible to see in Fig. 6 and Fig. SI3 good agreement between the simulated results (red solid lines) and the experimental ones (circles) obtained by femtosecond wavelength-tunable HRS technique. For molecule C1, as can be noted in Table I, only two photophysical parameters were essential to be used in Eq. (1) because only one excited state influences the incoherent second harmonic generated at the measured spectral region. For C4, and also C2, C3, and C5 molecules, besides μ_{01} and $\Delta\mu_{01}$, μ_{02} and μ_{12} were needed in Eq. (2), being μ_{12} the only free parameter.

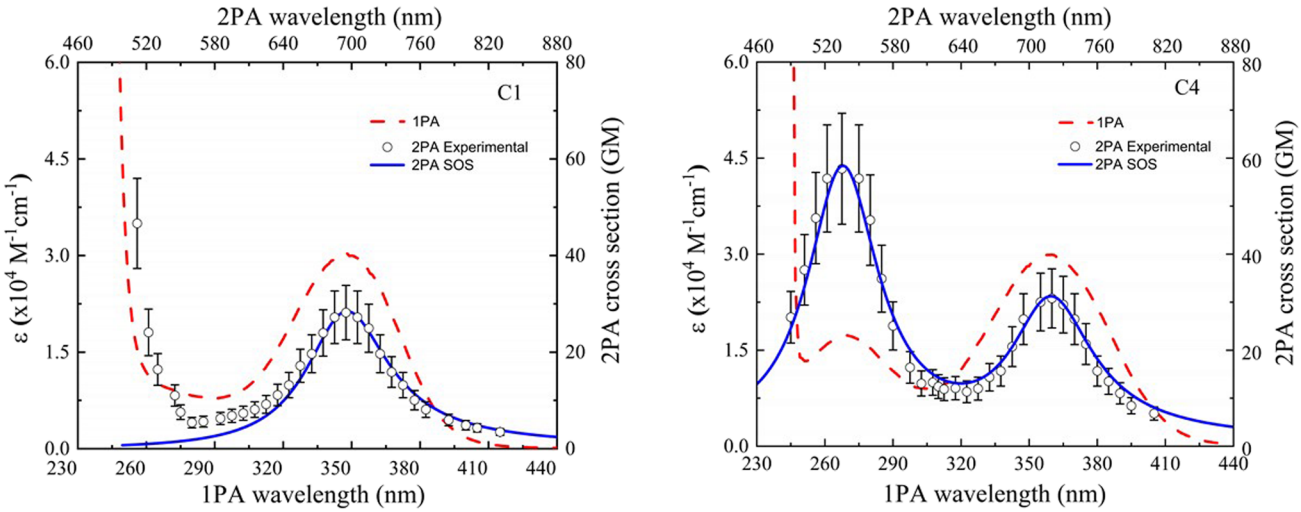

FIG. 5. Molar absorptivity spectra (red dashed lines), 2PA cross section (open circles), and the blue solid lines represent the adjustment using the SOS approach for C1 and C4 molecules.

TABLE I. Dipole moments (μ and $\Delta\mu$) and resonance enhancement factors (R_{1PA} and R_{2PA}) were obtained from 1PA and 2PA and employed in the SOS approach.

	C1	C2	C3	C4	C5
μ_{01} (D)	7.9 ± 0.7	7.7 ± 0.7	8.0 ± 0.8	7.8 ± 0.7	7.9 ± 0.8
μ_{02} (D)	···	5.3 ± 0.6	5.8 ± 0.6	6.5 ± 0.7	4.7 ± 0.5
μ_{12} (D)	···	2.8 ± 0.4	2.6 ± 0.4	2.6 ± 0.4	2.8 ± 0.4
$\Delta\mu_{01}$ (D)	7.7 ± 0.7	7.5 ± 0.7	7.5 ± 0.5	7.6 ± 0.7	7.6 ± 0.7
$\Delta\mu_{02}$ (D)	···	8.6 ± 0.9	8.8 ± 0.9	9.5 ± 0.9	9.0 ± 0.9
R_{1PA} (750 nm)	1.8 ± 0.2	1.9 ± 0.2	1.9 ± 0.2	1.9 ± 0.2	1.9 ± 0.2
R_{2PA} (750nm)	10.8 ± 0.6	11.2 ± 0.6	12.4 ± 0.6	14.8 ± 0.8	10.1 ± 0.5

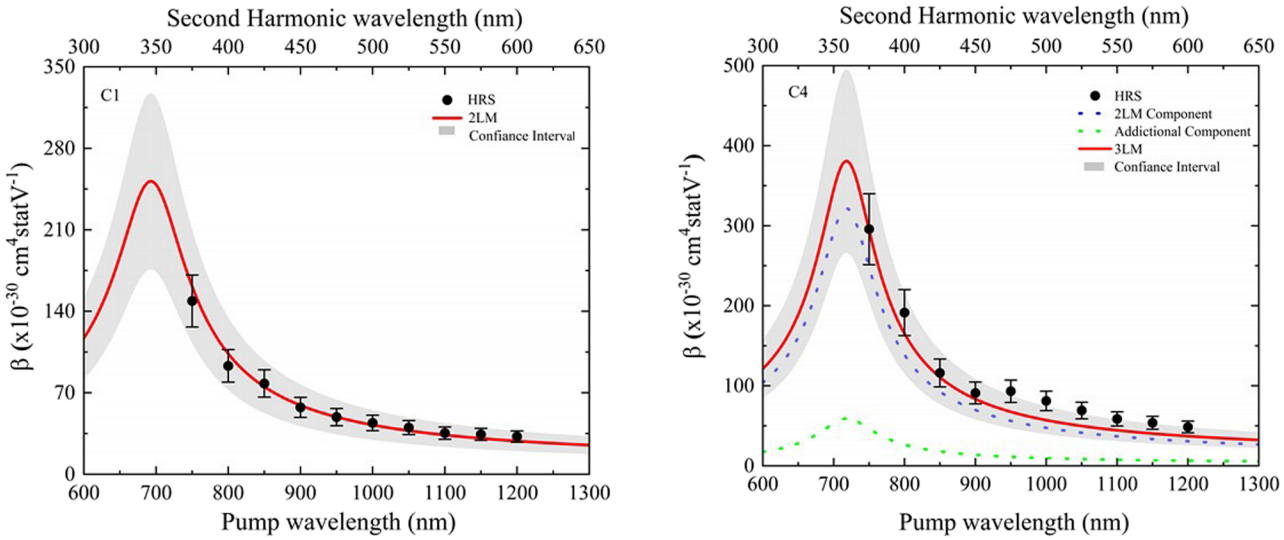

FIG. 6. Experimental dispersion of the first-order hyperpolarizability β (circles) with simulated results (red lines) and essential components (dashed lines) for C1 and C4 molecules.

For the C1 molecule, the first-order molecular hyperpolarizability calculated at 1300 nm is close in value to the experimental static first-order molecular hyperpolarizability, $\beta_0 \propto \Delta\mu_{01}\mu_{01}^2/(\hbar\omega_{01})^2$, which is essentially determined by $\Delta\mu_{01}$ and μ_{01} photophysical parameters. As the wavelengths get shorter, the dynamical term, represented by the second squared brackets in Eq. (1), starts to be relevant because the denominator shows two resonance enhancement effects for the measured spectral region, one at $R_{1PA}(\omega_{01} - \omega)$ and the other at $R_{2PA}(\omega_{01} - 2\omega)$. As can be seen, the former, the one photon resonance term, is significant when the incident laser frequency is approximately the same as the transition frequency of the first excited state ($\omega_{01} \cong \omega$), which, in our case, is far from 750 nm. Thus, this term contributes as a minimal value at the measured spectral region (see Table I). Therefore, the latter becomes the more significant to describe the enhancement of the first-order molecular hyperpolarizability at the 750 up to 900 nm spectral region. In this case, when the incident laser frequency is approximately half of the transition frequency of the first excited state (a two-photon resonance term, $\omega \cong \omega_{01}/2$), R_{2PA} tends to $\omega_{01}/\Gamma_{01}(\Gamma_{01} \ll \omega_{01})$, enhancing the dynamical first-order molecular hyperpolarizability. However, it only acts when the 1PA transition is allowed by a 2PA as well, which is only expected in non-centrosymmetric materials. Thus, the enhancement observed in the C1 first-order molecular hyperpolarizability is triggered by a 2PA-allowed state, which imposes that $\Delta\mu_{01}$ is not null. The same explanation applies to the other molecules as well. However, in this case, in addition to having only one 1PA state, two 1PA states are playing the role behind the first-order molecular hyperpolarizability. Besides the two resonances described before, an extra 1PA resonance, $(\omega_{02}/(\omega_{02} - \omega - i\Gamma_{02}))$, emerges due to the 3LM approach. In addition, this term is significant when the incident laser frequency is approximately the same as the transition frequency of the second excited state ($\omega_{02} \cong \omega$), which, in our case, is far from 750 nm. Thus, this term also contributes as a minimal value at the measured spectral region.

Another intriguing topic is understanding the effect of ED/EW groups at β(λ) values. To support this explanation, two figures of merit (FOM) were elaborated from an experimental point of view, as shown in Fig. 7. Figure 7(a) brings up the values of β for 750 nm (circles in blue), 850 nm (circles in green), 1000 nm (circles in red),

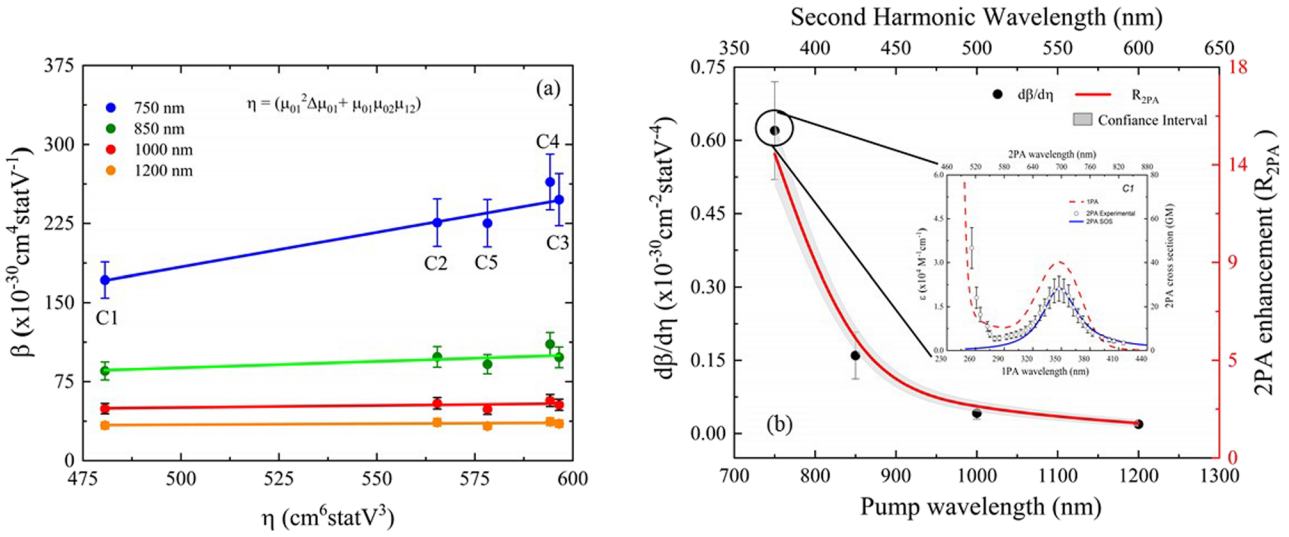

FIG. 7. (a) Colored circles represent the experimental values of (β) as a function of η for wavelengths at 750, 850, 1000, and 1200 nm for all molecules studied. The respective solid lines represent the linear fit that predicts the β values as a function of η. (b) dβ/dη as a function of pump wavelength. Black circles represent the values of dβ/dη at the wavelength indicated in Fig. 7(a), and the red solid line is an eye guide for R_{2PA}.

and 1200 nm (circles in orange) as a function of η parameter and the respective linear fits. η is defined here as the parameter associated with the effective contribution of the magnitude of the dipole moments ($\eta = \mu_{01}{}^2\Delta\mu_{01} + \mu_{01}\mu_{02}\mu_{12}$) in β values and is implicitly connected with the strength of peripheral groups.[57–59] For all wavelengths, β(λ) grow linearly with η, with a stronger dependence for wavelengths closer to the 1PA band, as shown by the rising slope of the linear fits. This effect is relative to the proximity of the incident laser wavelength to twice the energy band wavelengths, being both states responsible, whereby this statement can be seen in Fig. 7(b). For values between 1000 and 1200 nm, the value of slopes is approximately the same. It can be explained by a majority contribution from the static first-order molecular hyperpolarizability given by $\beta_0 = \frac{3}{2}\left(\frac{\mu_{01}{}^2\Delta\mu_{01}}{(\hbar\omega_{01})^2} + \frac{\mu_{01}\mu_{02}\mu_{12}}{(\hbar\omega_{01})(\hbar\omega_{02})}\right)$, where, for the 2LM, just the first term in the brackets is computed. Additionally, a remarkable increase in the values of β occurs at shorter wavelengths, which is connected to the enhancement promoted by the dynamical term (R_{2PA}). Consequently, these results show that the insertion of EW/ED groups enhances the incoherent second harmonic scattering in regions near the 2PA resonance. In a mathematical idea, the slope ($d\beta/d\eta$) shows how the value of β is incremented by an increase of one unit of η. Therefore, with the FOM represented in Fig. 7(a), it is possible to predict that, for this class of molecules, β values originated by the inclusion of other peripheral atoms with different strengths of ED or EW groups. Section IV of the supplementary material shows all the fittings curves.

It is worth mentioning that the first-order molecular hyperpolarizability spectrum also allows for the determination of photophysical parameters, such as those shown in Table I. After the modeling, it was observed that the values for μ_{12} are equivalent to those determined by the 2PA approach. Thus, the photophysical parameters can be determined regardless of the nonlinear optical constant modeled, i.e., via first-order hyperpolarizability dispersion β(λ) or via 2PA cross-sectional spectra (σ_{2PA}), indicating the consistency of experiments with the simulated data. Finally, these nonfluorescent molecules combine satisfactory β values at the therapeutic window (650–800 nm) and high biocompatibility ideal for applications in exogenous probes to Second Harmonic Generation (SHG) microscopy at biological tissues.[60–63]

IV. FINAL REMARKS

HRS measurements were performed on five samples from cinnamylidene acetophenone derivatives in a broad spectral range of 750–1200 nm, in which modeling of β dispersion was used to corroborate the experimental data. The β experimental dispersion near 1PA resonance showed a significant disparity depending on the EW or ED in the peripheral structure. The molecule C4, which has the highest β value at 750 nm ($\beta_{C4} = 295 \times 10^{-30}$ cm^4 statV^{-1}) compared to C1 ($\beta_{C1} = 148 \times 10^{-30}$ cm^4 statV^{-1}), shows an approximately twofold increase in its value, demonstrating the importance of understanding the effects of adding ED and EW groups to the molecular structure. In our study, we concluded that the addition of ED and EW groups leads to the substantial contribution of the higher energy electronic state on the increase of β. This effect was quantified through FOM-β, which is implicitly connected with the strength of ED or EW groups.

Furthermore, the β dispersion obtained through the modeling has presented considerable agreement with the experimental ones. It was shown that the photophysical parameters obtained separately by the SOS approach for 2PA or β display the same values, confirming the reliability of our method. Finally, we show that the β value is significantly enhanced by one order of magnitude due to the

2PA resonance. Such interesting outcomes may guide the synthesis of novel molecules with remarkable first-order hyperpolarizability with potential applications in SHG microscopy.

SUPPLEMENTARY MATERIAL

See the supplementary material for the details of Z-scan technique and the experimental and phenomenological 2PA cross-sectional spectra for C2, C3, and C5 molecules; description of the External Reference Method (ERM) to calculate experimentally the β(λ) values and the results for the dispersion of C2, C3, and C5 molecules; the linear absorption and Gaussian decomposition of all molecules; the equation of FOM [Fig. 7(a)] to predict the β values for other EW/ED groups; and, finally, the simplified equations to the SOS approach for a phenomenological determination of β(λ) values.

ACKNOWLEDGMENTS

The authors acknowledge the financial support from FAPESP (Fundação de Amparo à Pesquisa do Estado de São Paulo, Grant Nos. 2011/12399-0, 2015/20032-0 2016/20886-1, and 2018/11283-7), FAPEMIG (Fundação de Amparo à Pesquisa do Estado de Minas Gerais, Grant No. APQ-01469-18), CNPq (Conselho Nacional de Desenvolvimento Científico e Tecnológico, Grant No. 425180/2018-2), Coordenação de Aperfeiçoamento de Pessoal de Nível Superior (CAPES) Finance Code 001, Army Research Laboratory (Grant No. W911NF2110362), and Air Force Office of Scientific Research (Grant No. FA9550-12-1-0028).

AUTHOR DECLARATIONS

Conflict of Interest

The authors have no conflicts to disclose.

Author Contributions

Carlos H. D. dos Santos: Conceptualization (equal); Data curation (lead); Formal analysis (lead); Investigation (equal); Methodology (equal); Validation (equal); Writing – original draft (equal); Writing – review & editing (equal). **Leandro H. Zucolotto Cocca**: Data curation (supporting); Formal analysis (supporting); Methodology (supporting); Visualization (equal); Writing – original draft (equal). **André Gasparotto Pelosi**: Data curation (supporting); Formal analysis (supporting); Methodology (supporting); Visualization (supporting); Writing – original draft (equal). **Vasco F. Batista**: Methodology (equal); Validation (supporting); Visualization (supporting); Writing – original draft (supporting). **Diana C. G. A. Pinto**: Methodology (equal); Validation (supporting); Visualization (supporting); Writing – original draft (supporting). **M. Amparo F. Faustino**: Methodology (supporting); Validation (equal); Visualization (equal); Writing – original draft (supporting); Writing – review & editing (equal). **Marcelo G. Vivas**: Investigation (equal); Supervision (supporting); Validation (equal); Visualization (equal); Writing – original draft (supporting); Writing – review & editing (equal). **Jonathas de Paula Siqueira**: Methodology (equal); Validation (supporting); Visualization (supporting); Writing – original draft (equal); Writing – review & editing (supporting). **Cleber R. Mendonça**: Validation (equal); Visualization (equal); Writing – original draft (supporting); Writing – review & editing (equal). **Leonardo De Boni**: Conceptualization (lead); Investigation (equal); Methodology (lead); Supervision (lead); Writing – original draft (equal); Writing – review & editing (lead).

DATA AVAILABILITY

The data that support the findings of this study are available from the corresponding author upon reasonable request.

REFERENCES

[1]J. Liu, C. Ouyang, F. Huo, W. He, and A. Cao, "Progress in the enhancement of electro-optic coefficients and orientation stability for organic second-order nonlinear optical materials," Dyes Pigm. **181**, 108509 (2020).
[2]Y. Yan, Y. Yuan, B. Wang, V. Gopalan, and N. C. Giebink, "Sub-wavelength modulation of χ(2) optical nonlinearity in organic thin films," Nat. Commun. **8**(1), 14269 (2017).
[3]C. Yuan, X. Li, S. Semin, Y. Feng, T. Rasing, and J. Xu, "Chiral lead halide perovskite nanowires for second-order nonlinear optics," Nano Lett. **18**(9), 5411–5417 (2018).
[4]D. Chen, H. R. Fetterman, A. Chen, W. H. Steier, L. R. Dalton, W. Wang, and Y. Shi, "Demonstration of 110 GHz electro-optic polymer modulators," Appl. Phys. Lett. **70**(25), 3335–3337 (1997).
[5]M. Lee, H. E. Katz, C. Erben, D. M. Gill, P. Gopalan, J. D. Heber, and D. J. McGee, "Broadband modulation of light by using an electro-optic polymer," Science **298**(5597), 1401–1403 (2002).
[6]C. Kieninger, Y. Kutuvantavida, D. L. Elder, S. Wolf, H. Zwickel, M. Blaicher, J. N. Kemal, M. Lauermann, S. Randel, W. Freude, L. R. Dalton, and C. Koos, "Ultra-high electro-optic activity demonstrated in a silicon-organic hybrid modulator," Optica **5**(6), 739 (2018).
[7]A. Divochiy, F. Marsili, D. Bitauld, A. Gaggero, R. Leoni, F. Mattioli, A. Korneev, V. Seleznev, N. Kaurova, O. Minaeva, G. Gol'tsman, K. G. Lagoudakis, M. Benkhaoul, F. Lévy, and A. Fiore, "Superconducting nanowire photon-number-resolving detector at telecommunication wavelengths," Nat. Photonics **2**(5), 302–306 (2008).
[8]C. C. Corredor, Z.-L. Huang, and K. D. Belfield, "Two-photon 3D optical data storage via fluorescence modulation of an efficient fluorene dye by a photochromic diarylethene," Adv. Mater. **18**(21), 2910–2914 (2006).
[9]J. Campo, A. Painelli, F. Terenziani, T. Van Regemorter, D. Beljonne, E. Goovaerts, and W. Wenseleers, "First hyperpolarizability dispersion of the octupolar molecule crystal violet: Multiple resonances and vibrational and solvation effects," J. Am. Chem. Soc. **132**(46), 16467–16478 (2010).
[10]S. F. Hubbard, R. G. Petschek, and K. D. Singer, "Spectral content and dispersion of hyper-Rayleigh scattering," Opt. Lett. **21**(21), 1774 (1996).
[11]J. Campo, F. Desmet, W. Wenseleers, and E. Goovaerts, "Highly sensitive setup for tunable wavelength hyper-Rayleigh scattering with parallel detection and calibration data for various solvents," Opt. Express **17**(6), 4587 (2009).
[12]D. M. Bishop and D. W. De Kee, "The frequency dependence of nonlinear optical processes," J. Chem. Phys. **104**(24), 9876–9887 (1996).
[13]D. M. Bishop, "Explicit nondivergent formulas for atomic and molecular dynamic hyperpolarizabilities," J. Chem. Phys. **100**(9), 6535–6542 (1994).
[14]D. M. Bishop, "General dispersion formulas for molecular third-order nonlinear optical properties," J. Chem. Phys. **90**(6), 3192–3195 (1989).
[15]R. D. Fonseca, M. G. Vivas, D. L. Silva, G. Eucat, Y. Bretonnière, C. Andraud, L. De Boni, and C. R. Mendonça, "First-order hyperpolarizability of triphenylamine derivatives containing cyanopyridine: Molecular branching effect," J. Phys. Chem. C **122**(3), 1770–1778 (2018).

[16]N. W. Song, T.-I. Kang, S. C. Jeoung, S.-J. Jeon, B. R. Cho, and D. Kim, "Improved method for measuring the first-order hyperpolarizability of organic NLO materials in solution by using the hyper-Rayleigh scattering technique," Chem. Phys. Lett. **261**(3), 307–312 (1996).
[17]K. Clays and A. Persoons, "Hyper-Rayleigh scattering in solution," Phys. Rev. Lett. **66**(23), 2980–2983 (1991).
[18]P. L. Franzen, L. Misoguti, and S. C. Zilio, "Hyper-Rayleigh scattering with picosecond pulse trains," Appl. Opt. **47**(10), 1443 (2008).
[19]E. S. Gonçalves, L. H. Z. Cocca, W. W. R. Araujo, K. Parekh, C. L. P. Oliveira, J. P. Siqueira, C. R. Mendonça, L. De Boni, and A. M. Figueiredo Neto, "Influence of magnetic field on the two-photon absorption and hyper-Rayleigh scattering of manganese–zinc ferrite nanoparticles," J. Phys. Chem. C **124**(12), 6784–6795 (2020).
[20]P. Kaatz and D. P. Shelton, "Polarized hyper-Rayleigh light scattering measurements of nonlinear optical chromophores," J. Chem. Phys. **105**(10), 3918–3929 (1996).
[21]G. Berkovic, G. Meshulam, and Z. Kotler, "Measurement and analysis of molecular hyperpolarizability in the two-photon resonance regime," J. Chem. Phys. **112**(9), 3997–4003 (2000).
[22]J. Zhu, C. Lu, Y. Cui, C. Zhang, and G. Lu, "Two-photon resonant hyperpolarizability of an H-shaped molecule studied by wavelength-tunable hyper-Rayleigh scattering," J. Chem. Phys. **133**(24), 244503 (2010).
[23]J. M. F. Custodio, F. Gotardo, W. F. Vaz, G. D. C. D'Oliveira, L. R. de Almeida, R. D. Fonseca, L. H. Z. Cocca, C. N. Perez, A. G. Oliver, L. de Boni, and H. B. Napolitano, "Benzenesulfonyl incorporated chalcones: Synthesis, structural and optical properties," J. Mol. Struct. **1208**, 127845 (2020).
[24]K. Pielak, F. Bondu, L. Sanguinet, V. Rodriguez, B. Champagne, and F. Castet, "Second-order nonlinear optical properties of multiaddressable indolinooxazolidine derivatives: Joint computational and hyper-Rayleigh scattering investigations," J. Phys. Chem. C **121**(3), 1851–1860 (2017).
[25]F. Castet, V. Rodriguez, J.-L. Pozzo, L. Ducasse, A. Plaquet, and B. Champagne, "Design and characterization of molecular nonlinear optical switches," Acc. Chem. Res. **46**(11), 2656–2665 (2013).
[26]F. Castet, M. Blanchard-Desce, F. Adamietz, Y. M. Poronik, D. T. Gryko, and V. Rodriguez, "Experimental and theoretical investigation of the first-order hyperpolarizability of octupolar merocyanine dyes," ChemPhysChem **15**(12), 2575–2581 (2014).
[27]M. Gonçalves Vivas, J. Leandro De Sousa, L. De Boni, M. Schiavon, and C. Mendonca, "Observation of distinct two-photon transition channels in CdTe quantum dots in a regime of very strong confinement," Materials **10**(4), 363 (2017).
[28]E. M. P. Silva, T. Melo, B. C. Sousa, D. I. S. P. Resende, L. M. Magalhães, M. A. Segundo, A. M. S. Silva, and M. R. M. Domingues, "Do cinnamylideneacetophenones have antioxidant properties and a protective effect toward the oxidation of phosphatidylcholines?," Eur. J. Med. Chem. **121**, 331–337 (2016).
[29]S. E. Chuang, M. L. Kuo, C. H. Hsu, C. R. Chen, J. K. Lin, G. M. Lai, C. Y. Hsieh, and A. L. Cheng, "Curcumin-containing diet inhibits diethylnitrosamine-induced murine hepatocarcinogenesis," Carcinogenesis **21**(2), 331–335 (2000).
[30]K. Piwocka, A. Bielak-mijewska, and E. Sikora, "Curcumin induces caspase-3-independent apoptosis in human multidrug-resistant cells," Ann. N. Y. Acad. Sci. **973**, 250–254 (2002).
[31]A. A. Nanji, K. Jokelainen, G. L. Tipoe, A. Rahemtulla, P. Thomas, and A. J. Dannenberg, "Curcumin prevents alcohol-induced liver disease in rats by inhibiting the expression of NF-κB-dependent genes," Am. J. Physiol.: Gastrointest. Liver Physiol. **284**(2), G321 (2003).
[32]A. Duvoix, R. Blasius, S. Delhalle, M. Schnekenburger, F. Morceau, E. Henry, M. Dicato, and M. Diederich, "Chemopreventive and therapeutic effects of curcumin," Cancer Lett. **223**(2), 181–190 (2005).
[33]F. Zhang, N. K. Altorki, J. R. Mestre, K. Subbaramaiah, and A. J. Dannenberg, "Curcumin inhibits cyclooxygenase-2 transcription in bile acid- and phorbol ester-treated human gastrointestinal epithelial cells," Carcinogenesis **20**(3), 445–451 (1999).
[34]K. Singletary, C. MacDonald, M. Wallig, and C. Fisher, "Inhibition of 7,12-dimethylbenz[a]anthracene (DMBA)-induced mammary tumorigenesis and DMBA-DNA adduct formation by curcumin," Cancer Lett. **103**(2), 137–141 (1996).
[35]C. Polaquini, G. Torrezan, V. Santos, A. Nazaré, D. Campos, L. Almeida, I. Silva, H. Ferreira, F. Pavan, C. Duque, and L. Regasini, "Antibacterial and antitubercular activities of cinnamylideneacetophenones," Molecules **22**(10), 1685 (2017).
[36]D. J. Weldon, M. D. Saulsbury, J. Goh, L. Rowland, P. Campbell, L. Robinson, C. Miller, J. Christian, L. Amis, N. Taylor, C. Dill, W. Davis, S. L. Evans, and E. Brantley, "One-pot synthesis of cinnamylideneacetophenones and their in vitro cytotoxicity in breast cancer cells," Bioorg. Med. Chem. Lett. **24**(10), 3381–3384 (2014).
[37]W. Bartkowiak, R. Zaleśny, and J. Leszczynski, "Relation between bond-length alternation and two-photon absorption of a push–pull conjugated molecules: A quantum-chemical study," Chem. Phys. **287**(1–2), 103–112 (2003).
[38]M. G. Vivas, D. L. Silva, J. Malinge, M. Boujtita, R. Zaleśny, W. Bartkowiak, H. Ågren, S. Canuto, L. De Boni, E. Ishow, and C. R. Mendonca, "Molecular structure – optical property relationships for a series of non-centrosymmetric two-photon absorbing push-pull triarylamine molecules," Sci. Rep. **4**(1), 4447 (2015).
[39]B. J. Orr and J. F. Ward, "Perturbation theory of the non-linear optical polarization of an isolated system," Mol. Phys. **20**(3), 513–526 (1971).
[40]M. G. Vivas, L. De Boni, T. M. Cooper, and C. R. Mendonca, "Interpreting strong two-photon absorption of PE3 platinum acetylide complex: Double resonance and excited state absorption," ACS Photonics **1**(2), 106–113 (2014).
[41]L. P. Hammett, "The effect of structure upon the reactions of organic compounds. Benzene derivatives," J. Am. Chem. Soc. **59**(1), 96–103 (1937).
[42]A. LÉvai, T. Patonay, A. M. S. Silva, D. C. G. A. Pinto, and J. A. S. Cavaleiro, "Synthesis of 3-aryl-5-styryl-2-pyrazolines by the reaction of (E,E)-cinnamylideneacetophenones with hydrazines and their oxidation into pyrazoles," J. Heterocycl. Chem. **39**(4), 751–758 (2002).
[43]D. C. G. A. Pinto, A. M. S. Silva, A. Lévai, J. A. S. Cavaleiro, T. Patonay, and J. Elguero, "Synthesis of 3-benzoyl-4-styryl-2-pyrazolines and their oxidation to the corresponding pyrazoles," Eur. J. Org. Chem. **2000**(14), 2593–2599.
[44]R. W. Terhune, P. D. Maker, and C. M. Savage, "Measurements of nonlinear light scattering," Phys. Rev. Lett. **14**(17), 681–684 (1965).
[45]J. M. F. Custodio, G. D. C. D'Oliveira, F. Gotardo, L. H. Z. Cocca, L. de Boni, C. N. Perez, H. B. Napolitano, F. A. P. Osorio, and C. Valverde, "Second-order nonlinear optical properties of two chalcone derivatives: Insights from sum-over-states," Phys. Chem. Chem. Phys. **23**(10), 6128–6140 (2021).
[46]J. M. F. Custodio, F. Gotardo, W. F. Vaz, G. D. C. D'Oliveira, L. H. Z. Cocca, R. D. Fonseca, C. N. Perez, L. de Boni, and H. B. Napolitano, "Sulphonamide chalcones: Conformationally diverse yet optically similar," J. Mol. Struct. **1198**, 126896 (2019).
[47]L. F. Sciuti, L. M. G. Abegão, C. H. D. dos Santos, L. H. Zucolotto Cocca, R. G. M. da Costa, J. Limberger, L. Misoguti, C. R. Mendonça, and L. De Boni, "Modeling the first-order molecular hyperpolarizability dispersion from experimentally obtained one- and two-photon absorption," J. Phys. Chem. A **126**(14), 2152–2159 (2022).
[48]B. J. Orr and J. F. Ward, "Perturbation theory of the non-linear optical polarization of an isolated system," Mol. Phys. **20**(3), 513–526 (1971).
[49]J. L. Oudar and D. S. Chemla, "Hyperpolarizabilities of the nitroanilines and their relations to the excited state dipole moment," J. Chem. Phys. **66**, 2664–2668 (1977).
[50]R. Boyd, *Nonlinear Optics* (Academic Press, 2020).
[51]T. Verbiest, K. Clays, and V. Rodriguez, *Second-Order Nonlinear Optical Characterization Techniques* (CRC Press, 2009).
[52]G. J. T. Heesink, A. G. T. Ruiter, N. F. van Hulst, and B. Bölger, "Determination of hyperpolarizability tensor components by depolarized hyper Rayleigh scattering," Phys. Rev. Lett. **71**(7), 999–1002 (1993).
[53]J. M. F. Custodio, G. D. C. D'Oliveira, F. Gotardo, L. H. Z. Cocca, L. De Boni, C. Noda Perez, L. J. Q. Maia, C. Valverde, F. A. P. Osorio, and H. B. Napolitano, "Chalcone as potential nonlinear optical material: A combined theoretical, structural and spectroscopic study," J. Phys. Chem. A **123**, 5931 (2019).
[54]L. M. G. Abegão, F. A. Santos, R. D. Fonseca, A. L. B. S. Barreiros, M. L. Barreiros, P. B. Alves, E. V. Costa, G. B. Souza, M. A. R. C. Alencar, C. R. Mendonça, K. Kamada, L. De Boni, and J. J. Rodrigues, "Chalcone-based molecules: Experimental and theoretical studies on the two-photon absorption and molecular first hyperpolarizability," Spectrochim. Acta, Part A **227**, 117772 (2020).

[55]L. H. Zucolotto Cocca, A. G. Pelosi, S. Piguel, C. R. Mendonça, and L. D. Boni, "Enhancement of optical properties of new purine nucleobases containing electron-donating and -withdrawing peripheral groups," J. Photochem. Photobiol., B **234**, 112524 (2022).
[56]M. G. Vivas, L. De Boni, and C. R. Mendonça, *Molecular and Laser Spectroscopy* (Elsevier, 2018), pp. 165–191.
[57]M. Charton, "Application of the Hammett equation to substituent effects on π donors in charge-transfer complex formation. II. Multiply substituted donors," J. Org. Chem. **31**(9), 2996–3000 (1966).
[58]N. Sadlej-Sosnowska and M. Kijak, "Excited state substituent constants: To Hammett or not?," Struct. Chem. **23**(2), 359–365 (2012).
[59]C. Hansch, A. Leo, and R. W. Taft, "A survey of Hammett substituent constants and resonance and field parameters," Chem. Rev. **91**(2), 165–195 (1991).
[60]M. Fecková, P. le Poul, F. Bureš, F. Robin-le Guen, and S. Achelle, "Nonlinear optical properties of pyrimidine chromophores," Dyes Pigm. **182**, 108659 (2020).
[61]N. Kato, "Optical second harmonic generation microscopy: Application to the sensitive detection of cell membrane damage," Biophys. Rev. **11**(3), 399–408 (2019).
[62]V. V. Dudenkova, M. V. Shirmanova, M. M. Lukina, F. I. Feldshtein, A. Virkin, and E. V. Zagainova, "Examination of collagen structure and state by the second harmonic generation microscopy," Biochemistry (Moscow) **84**(S1), 89–107 (2019).
[63]G. Cox, E. Kable, A. Jones, I. Fraser, F. Manconi, and M. D. Gorrell, "3-Dimensional imaging of collagen using second harmonic generation," J. Struct. Biol. **141**(1), 53–62 (2003).